


Reversible nonvolatile control of anomalous valley Hall effect in a multiferroic van der Waals heterostructure

Chengan Lei,¹ Xinru Li^{1,2,*}, Yandong Ma,² and Zhao Qian^{1,†}

¹Key Laboratory for Liquid-Solid Structural Evolution and Processing of Materials (Ministry of Education), and School of Materials Science and Engineering, Shandong University, Jinan 250061, China

²School of Physics, State Key Laboratory of Crystal Materials, Shandong University, Jinan 250100, China

 (Received 18 May 2023; revised 4 September 2023; accepted 3 October 2023; published 26 October 2023)

Controlling the anomalous valley Hall (AVH) effect by external means is crucial for valleytronic devices in practical applications; however, most of the previously proposed control approaches are either irreversible or volatile. Here, we present a general scheme for achieving nonvolatile electrical control of the AVH effect based on multiferroic van der Waals heterostructure. Using density functional theory calculations and $\mathbf{k} \cdot \mathbf{p}$ model analysis, we further demonstrate the feasibility of this design principle by stacking ferromagnetic monolayer VSe₂ on ferroelectric monolayer Al₂S₃. The reversible switching of AVH can be finely manipulated by reversing the ferroelectric polarization of Al₂S₃ via electric field. The regulated AVH state of VSe₂ can be stably preserved due to the ferroelectric nonvolatility of Al₂S₃. In addition, the sign of valley polarization can be simultaneously inverted by reversing ferroelectric polarization. Our results not only provide the basis for an intrinsic ferroelectricity controlled ferrovalley, but also uncover an outstanding candidate for realizing bidirectional and nonvolatile switching valleytronic devices.

DOI: [10.1103/PhysRevB.108.155431](https://doi.org/10.1103/PhysRevB.108.155431)

I. INTRODUCTION

Exploring new quantum degrees of freedom and finding effective control approaches potentially open up a new paradigm for the next-generation nanoelectronics devices [1]. For instance, in certain crystals with two or more degenerate but inequivalent energy extrema in momentum space, carriers can endow a valley degree of freedom in addition to conventional charge and spin [2,3]. Because the valleys are well separated by a large momentum space, intervalley interactions are expected to be suppressed [4], which can provide enough time to manipulate the carriers and complete the designed function. As a result, the valley has been proposed to encode, process, and store information, leading to a new technology known as valleytronics [5–11]. To date, manipulating valley-related effects has become an exciting new frontier for both fundamental research and practical applications.

The valley-dependent physical quantities, such as Berry curvature and orbital magnetic moment [12,13], provide powerful handles to address and control the valley-related effects. For instance, encoding Berry curvature with valley degrees of freedom in valley-polarized materials can lead to new types of Hall effect called the anomalous valley Hall (AVH) effect [14,15]. The emergence of two-dimensional (2D) materials, particularly hexagonal lattices with valley polarization and strong spin-orbit coupling (SOC), has reinvigorated the AVH effect field in the past several years [16–19]. For example, the electrical control of the AVH effect was confirmed in an antiferrovalley bilayer VSe₂ system [20], which had applications in all-electric reading and writing memory

devices. Very recently, on the basis of inversion symmetric single-layer lattices, the AVH effect in bilayer $T\text{--FeCl}_2$ was theoretically identified, which can be controlled by the ferroelectric switching [21]. In addition, the AVH effect in antiferromagnetic monolayer MnPSe₃ was proposed, which was well dependent on the stacking pattern with monolayer Sc₂CO₂ [22]. The electric field and ferroelectric polarization are also identified as effective methods to control valleytronics in multiferroic heterostructure, such as in AgBiP₂S₆/CrBr₃ [23], WSe₂/VSe₂ [24], and CrOX/In₂Se₃ [25] multiferroic heterostructure. All these elaborate design principles expand the candidates with AVH effect and enrich the research for achieving the electrical control of the AVH effect in 2D materials. However, it is still challenging to finely filter carriers with certain spin and valley indexes in one specific system, and realize reversible and nonvolatile control of the AVH effect.

In this work, we show that multiferroic (ferrovalley/ferroelectric) van der Waals heterostructures provide an embodiment to realize reversible nonvolatile control of valleytronic devices. We further predict a real heterostructure of VSe₂/Al₂S₃ to demonstrate the feasibility of this design principle through first-principles calculations and $\mathbf{k} \cdot \mathbf{p}$ model analysis. The spontaneous valley polarization of VSe₂ can be changed from valence band maximum (VBM) to conduction band minimum (CBM) when the ferroelectric polarization of Al₂S₃ is switched via a short-term voltage. Thus, the signs of Hall voltage in the AVH effect can be precisely controlled based on the direction of ferroelectric polarization. These results indicate that reversible and nonvolatile electrical control of the AVH effect can be realized by ferroelectric switching, which is very interesting for designing next-generation all-electric valleytronic devices.

*lixr@sdu.edu.cn

†qianzhao@sdu.edu.cn

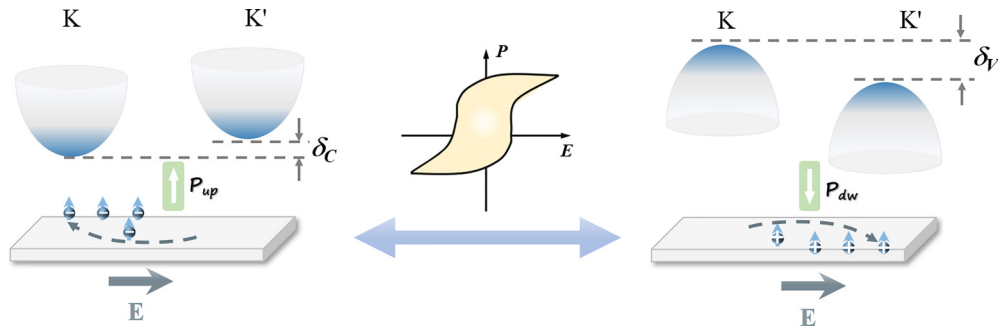


FIG. 1. Design principle based on multiferoic heterostructure. Diagrams of band structures around the K and K' valleys and FE-controlled AVH effect under in-plane electric field. The white arrows represent the direction of FE polarization. The holes/electrons are denoted by white $+/-$ symbols. The δ_C (δ_V) is the energy difference of CBM (VBM) between K and K' valleys.

II. METHODS

Our first-principles calculations were performed based on the density functional theory (DFT) [26] by the Vienna *ab initio* simulation package (VASP) [27]. The generalized gradient approximation (GGA) in the form of the Perdew-Burke-Ernzerhof (PBE) functional [28,29] was employed to treat the exchange-correlation effect among electrons. The projector augmented wave (PAW) method [30,31] was employed to describe the ionic potential. The plane-wave cutoff energy was set to be 520 eV. The convergence criteria of total energy and force were set as 10^{-5} eV and 0.01 eV/Å, respectively. The Brillouin zone was sampled using Γ -centered Monkhorst-Pack [32] k -point grids of $9 \times 9 \times 1$. A vacuum space of 20 Å was inserted along the z direction to eliminate the spurious interactions between adjacent layers. The Heyd-Scuseria-Ernzerhof (HSE06) [33] hybrid functional was employed to obtain accurate band structures. A dipole correction [34] was considered. The interlayer van der Waals interaction was described by the DFT-D2 [35] method. For the calculations of Berry curvature, the maximally localized Wannier functions (MLWFs) implemented in the WANNIER90 package are employed [36].

III. RESULTS AND DISCUSSION

The realization of the AVH effect hinges on optional control of valley polarization. In principle, the breaking of both spatial inversion symmetry and time-reversal symmetry is required for valley polarization. Without losing any generality, we take the well-known ferrovalley monolayer VSe₂ [14], shown in Fig. S1(a) in the Supplemental Material [37], as an example to discuss our design principle. It is worth noting that 2D H -phase VSe₂ has been successfully synthesized in experiment [38]. Monolayer VSe₂ has D_{3h} symmetry and a ferromagnetic ground state. In this regard, both inversion symmetry and time-reversal symmetry are broken, which can lead to nonzero Berry curvature with unequal size and opposite sign at the K and K' valleys. The band structure of monolayer VSe₂ with SOC is shown in Fig. S2 [37]. The energy degeneracy between two valleys is lifted and valley polarization appears. When an external in-plane electric field is applied, Bloch electrons from one valley (K/K') acquire transverse velocities toward the side under the effective magnetic field

generated by Berry curvature at K/K' , and the AVH effect can be generated. Because the valley polarization of monolayer VSe₂ originates from the spin-orbit coupling coexisting with the inherent exchange interaction [14], an external magnetic field can be applied to tune the valley polarization, and then the sign of the AVH effect. Compared with the control of valley polarization by the energy-intensive magnetic way, alternative manipulation via a reversible and nonvolatile electrical method is highly desirable.

To this end, 2D ferroelectric (FE) materials with two stable and electrically switchable polarized states [39,40] are ideal candidates for precise control of ferrovalley materials. Note that the reversed polarized state will be retained even if the external electrical control is removed. It means that electrical switching between these two polarized states is nonvolatile. In principle, if the ferrovalley monolayer VSe₂ is placed on the top of a FE substrate, the valley polarization and AVH can be potentially modulated by ferroelectric switching, achieving an electrically controlled AVH effect. Our proposed design principle is schematically illustrated in Fig. 1. The valley polarization of VSe₂ can be changed from VBM to CBM when the polarization direction is reversed. Such a transition is accompanied by the valley of the VBM or CBM being submerged in the trivial bands, while for the case under doping, it will not lead to the submersion of valleys in the trivial bands. More importantly, the sign of the AVH effect can be well tuned with reversibility and nonvolatility by the FE substrate, which cannot be realized by tuning the doping type.

Based on the above design principle, we consider 2D Al₂S₃ as a FE substrate to tune the AVH effect of VSe₂. Its crystal structures with two polarizations are presented in Figs. S1(b) and S1(c) [37]. The stable 2D Al₂S₃ monolayer shows quintuple layer structures of S-Al-S-Al-S with space group $P3m1$. The calculated lattice parameter of Al₂S₃ is 3.59 Å, which agrees well with a previous report [41]. Due to the asymmetric displacement of atoms in the central S layer, Al₂S₃ exhibits ferroelectricity with reversible spontaneous electric polarization in out of plane orientations. The FE polarization states are denoted as P_{up} and P_{dw} when the middle S atom is vertically aligned with the upper and lower Al layers, respectively. Al₂S₃ belongs to the well-known ferroelectric family of In₂Se₃, which has been experimentally reported to be a room temperature FE [42,43]. The band structure without spin-orbital coupling (SOC) of 2D Al₂S₃ indicates

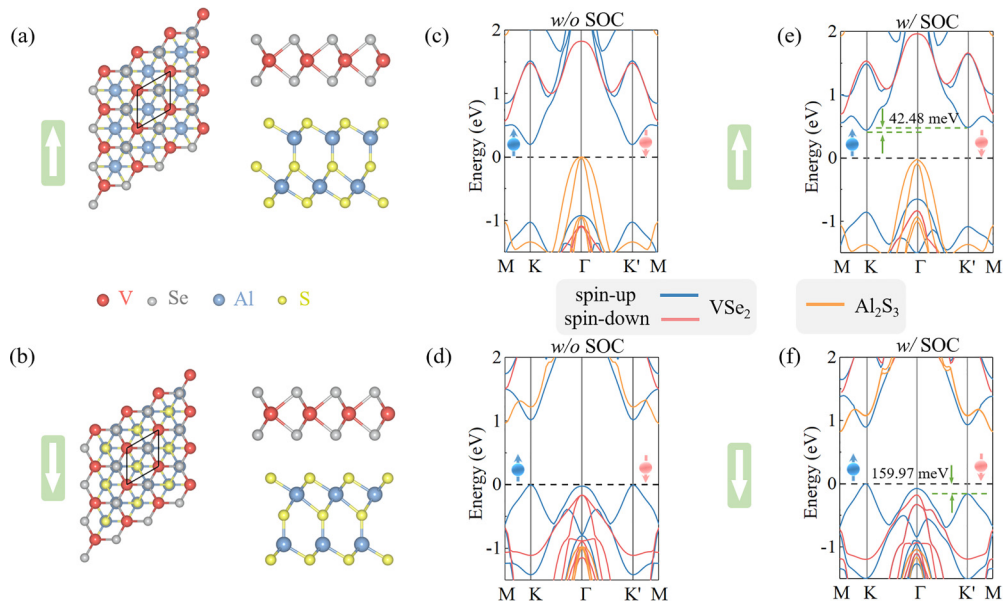


FIG. 2. Crystal structures of (a) type- V_{up} and (b) type- V_{dw} configurations from top and side views. Black rhombus in (a), (b) marks the unit cells. Band structures of (c) type- V_{up} and (d) type- V_{dw} configurations without SOC. Band structures of (e) type- V_{up} and (f) type- V_{dw} configurations with SOC. White arrows show the FE polarization direction. Blue and red lines represent the contributions from spin-up and spin-down channels of VSe_2 , and orange lines denote the contributions from Al_2S_3 . The Fermi level is set to zero.

that it is a semiconductor with indirect band gap 2.97 eV; see Fig. S1(e) [37]. The VBM is located along the K - Γ line of the Brillouin zone and the CBM at the Γ point. We also consider the SOC effect. However, it modifies the band structure of Al_2S_3 slightly; see Fig. S1(f) [37].

To construct VSe_2/Al_2S_3 multiferroic heterostructure, the unit cell of 2D Al_2S_3 is adopted to match the unit cell of 2D VSe_2 . The small lattice mismatch of 3.6% between them suggests the experimental fabrication of such heterostructure would be easily achieved. Here, six possible stacking configurations are considered for two polarized states, as shown in Figs. S3(a) and S3(b) [37]. To confirm the energetically most stable stacking pattern, we calculate the relative energies of different structures (Table S1 [37]). It shows that the type V for two polarization directions is energetically lower than the other configurations. The obtained interlayer distances of type V are 3.18 Å (P_{up}) and 3.19 Å (P_{dw}), respectively, which are also smaller than other stacking patterns; see Table S1 [37]. More importantly, the ferromagnetic (FM) ground state of VSe_2 is maintained in the multiferroic heterostructure. Table S2 [37] lists the energies of different magnetic configurations. Meanwhile, for the magnetic moment, it is almost contributed by the V atom, which can be found in the spin-polarized charge densities (Fig. S4 [37]).

Next, we will take type V as an example to discuss the possibility of controlling valley polarization and the AVH effect. The top and side views of type-V heterostructure with P_{up} (type V_{up}) and P_{dw} (type V_{dw}) are shown in Figs. 2(a) and 2(b), respectively. The V (Se) atom of the VSe_2 layer is located above the S (Al) atom of the Al_2S_3 layer in type V. The energy difference between type V_{up} and type V_{dw} was found to be 0.043 eV. Their band structures without considering SOC are shown in Figs. 2(c) and 2(d). For the type- V_{up} configuration, it shows a semiconducting property with an indirect band gap of 0.20 eV. The VBM is located at the Γ point and the

CBM at the K point. The VBM and CBM are contributed by Al_2S_3 and the spin-up channel of VSe_2 , respectively, forming the typical staggered-gap (type II) band alignment. Clearly, the CBM holds two energetically degenerate valleys with the same spin components at K/K' ; see Fig. 2(c). Although the highest valence band still forms energy extrema at the K/K' points, a pair of valleys is submerged in the trivial bands of Al_2S_3 . As for the type- V_{dw} case, the band structure undergoes a major change. The indirect band gap is changed to 0.97 eV, which is larger than that of type V_{up} . The VBM is changed to the K point and the CBM to the M point; see Fig. 2(d). Although type-II band alignment is preserved, the band edge contributions are flipped compared with type V_{up} . As a result, the contributions of VBM and CBM are dominated by spin-up channel of VSe_2 and Al_2S_3 , respectively. In contrast to type V_{up} , the valleys of VBM are preserved well at the K/K' points, while the valleys in the lowest conduction band are submerged in the trivial bands of Al_2S_3 . As a matter of fact, these two valleys are inequivalent because of the intrinsic inversion symmetry breaking, and thus both type V_{up} and type V_{dw} are valleytronic candidates. It should be noted that the type-II band alignment is always preserved in these two heterostructures. This can be attributed to the different work functions and band gaps of the two materials. Based on former research [44], when $E_{g1} > \Delta W$, the two materials will not become metallic and tend to achieve type-II band alignment. Here, E_{g1} is defined as the band gap of the material whose surface in contact has a larger work function than that of the other material. ΔW is the work function difference between the two materials. For type- V_{up} configuration, the $E_{g1} = 1.02$ eV $>$ $\Delta W = 0.59$ eV. For type- V_{dw} configuration, the $E_{g1} = 2.97$ eV $>$ $\Delta W = 1.79$ eV. Therefore, these two heterostructures always hold type-II band alignment.

When we consider the SOC effect, as shown in Figs. 2(e) and 2(f), the valley spin splitting of VSe_2 is maintained

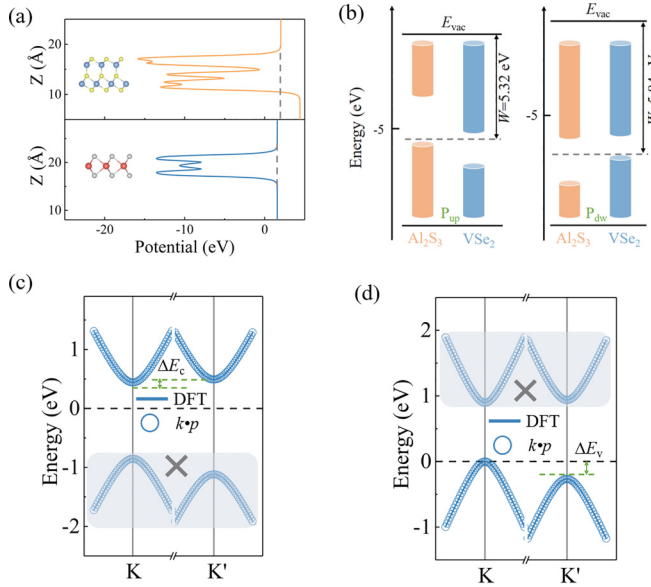


FIG. 3. (a) Plane-averaged electrostatic potentials of monolayer Al₂S₃ and VSe₂. (b) Band alignments of type-V_{up} and type-V_{dw} configurations with respect to the vacuum level. Low-energy band structures with SOC around the K/K' valleys for (c) type-V_{up} and (d) type-V_{dw} configurations calculated from DFT results (lines) and $k \cdot p$ model (circles). Gray shading represents the relative position of electronic states contributed by Al₂S₃ in heterostructures.

at K/K', but the energy levels of the valleys become non-degenerate, yielding the spontaneous valley polarizations. For the P_{up} (P_{dw}) case, the band gap is found to be 0.44 (0.83) eV. The spontaneous valley polarization of type V_{up} (type V_{dw}) in the CBM (VBM) is calculated to be $\Delta E_c = 42.48$ meV ($\Delta E_v = 159.97$ meV). These values are much larger than some experimentally demonstrated magnetic proximity systems (0.3–1.0 meV) [45] and available ferrovalley [46] materials, which can resist the annihilation of valley polarization caused by kinetic energy near room temperature (26 meV). Note that the valleys of VSe₂ in the VBM (CBM) at K/K' for type-V_{up} (type-V_{dw}) heterostructure are submerged in the trivial bands of Al₂S₃, restricting any potential utilizations. Thus, the effective response induced by valley polarization is switched from CBM to VBM under the ferroelectric polarization flipping. Such transition is also accompanied with the change of valley physics as well as the AVH effect. It means that the AVH effect can be well controllable by flipping the electric polarization of Al₂S₃, benefiting the development of reversible nonvolatile controllable valleytronic devices. This is different from that of VSe₂/Sc₂CO₂ heterostructure [47] wherein only the on-off switch of the AVH effect is realized through ferroelectricity.

The underlying mechanism of the ferroelectric control of the AVH effect was also explored. Note that monolayer Al₂S₃ is a FE crystal with an out of plane FE polarization; it can produce the external electric field, leading to the different potential energies on the two sides of the sample. As for monolayer VSe₂, the potential energy displays the same value. To identify this, the plane average electrostatic potentials of Al₂S₃ and VSe₂ are calculated, as shown in

Fig. 3(a). The potential energy difference of Al₂S₃ is 2.39 eV, while the value of VSe₂ is 0 eV. When the VSe₂ is deposited on the Al₂S₃ in two polarized states, the different band edges are formed due to the polarization field; see Fig. 3(b). Thus, the valley polarizations and signs of the AVH effect are changed correspondingly by flipping the electric polarization. For the P_{up} case, the bands from VSe₂ move downward driven by the polarization field, which results in the CBM and VBM of VSe₂ being lower than the CBM and VBM of the Al₂S₃ monolayer. Consequently, the CBM of the heterostructure is associated with the VSe₂, while the VBM comes from the Al₂S₃ monolayer. The valley polarization feature of VSe₂ in the CBM is preserved. In contrast, for the P_{dw} configuration, the energy bands of VSe₂ shift to higher energy since the polarization field is reversed. This change of energy level finally leads to the CBM (VBM) of the Al₂S₃ monolayer shifting below the CBM (VBM) of VSe₂. In this case, only the valley polarization of VSe₂ in the VBM can be used.

To further understand these properties, an effective $k \cdot p$ model is established here to characterize the low-energy band dispersions at K and K' valleys. Considering the orbital contributions of the band edges around the K and K' valleys, the electronic states $|\psi_c^\tau\rangle = |d_{z^2}\rangle$ and $|\psi_v^\tau\rangle = \frac{1}{\sqrt{2}}(|d_{x^2-y^2}\rangle + i\tau|d_{xy}\rangle)$ are adopted as basis functions, where $\tau = \pm 1$ represents the two nonequivalent points of the Brillouin zone and the subscript c/v indicates the conduction/valence band. For the pure monolayer VSe₂ without a FE substrate, the band gaps are located at valleys K and K' with C_{3h} point group symmetry. The $k \cdot p$ model can be employed [3,14,48] to well describe the electronic properties of VSe₂. For the VSe₂/Al₂S₃ heterostructures, the orbital contributions at the valleys are all dominated by d orbitals of V atoms in the VSe₂ layers. Following the previous works [47,49], the effect of the ferroelectric Al₂S₃ substrate in the $k \cdot p$ model is established by adding an external electrostatic field term H_E . The total Hamiltonian is given by $H_k = H_0 + H_{\text{SOC}} + H_{\text{ex}} + H_E$.

Here,

$$H_0(k) = \begin{bmatrix} \frac{\Delta}{2} + \varepsilon & t(\tau q_x - i q_y) \\ t(\tau q_x + i q_y) & -\frac{\Delta}{2} + \varepsilon \end{bmatrix}, \quad (1)$$

where Δ is the band gap in the valley, ε is the on-site energy, and t is the effective nearest-neighbor hopping integral.

The second term H_{SOC} originating from the SOC effect can be written as

$$H_{\text{SOC}} = \begin{bmatrix} \tau s \lambda_c & 0 \\ 0 & \tau s \lambda_v \end{bmatrix}, \quad (2)$$

where $s = \pm 1$ represents spin up and spin down, and $\lambda_c(v)$ represents the spin splitting due to the SOC effect.

The third term, H_{ex} , is the inherent exchange interaction of V ions:

$$H_{\text{ex}} = \begin{bmatrix} -sm_c & 0 \\ 0 & -sm_v \end{bmatrix}, \quad (3)$$

where $m_{c(v)}$ demonstrates the effective exchange splitting at the band edges.

The fourth term, H_E , is given by

$$H_E = \begin{bmatrix} \frac{U}{2} & 0 \\ 0 & \frac{U}{2} \end{bmatrix}, \quad (4)$$

where U is the potential induced by the FE layer.

The parameters of the model are listed in Table S3 [37]. The fitted bands around the K and K' valleys for type- V_{up} and type- V_{dw} configurations by the $\mathbf{k} \cdot \mathbf{p}$ model are illustrated in Figs. 3(c) and 3(d), which are close to the first-principles results. The valley polarization features of VSe_2 are well reproduced for the two configurations. This verifies the AVH effect is ferroelectrically controllable in the VSe_2/Al_2S_3 heterostructure by the polarized electric field of the FE substrate.

After identifying the design principle and underlying physics, we characterize the valley properties by Berry curvature, which is an important quantity in valleytronics. Because of the inversion symmetry breaking in our design systems, the charge carriers in the K and K' valleys exhibit a nonzero Berry curvature along the out of plane direction, which is the basis for realizing the AVH effect. The Berry curvatures are derived from the Kudo formula [50], which can be expressed as

$$\Omega(k) = - \sum_n \sum_{n' \neq n} f_n \frac{2\text{Im}\langle \psi_{nk} | v_x | \psi_{n'k} \rangle \langle \psi_{n'k} | v_y | \psi_{nk} \rangle}{(E_n - E_{n'})^2}. \quad (5)$$

Here, n and n' are the band indices, and f_n , $|\psi_{n(n')k}\rangle$, and $v_{x/y}$ are the Fermi-Dirac distribution function for the n th band, the Bloch wave function with eigenvalue $E_{n(n')}$, and the velocity operator of the Dirac electrons along the x/y directions. The corresponding Berry curvatures are displayed in Figs. 4(a) and 4(b). Obviously, the Berry curvatures around the K/K' valley have different absolute values and exhibit opposite signs, suggesting the robust valley-contrasting feature. Here, the valley polarization is switched from CBM to VBM by the reversal of ferroelectric polarization. Since the time-reversal operator changes the orbital part of the Bloch function to its complex conjugate and flips the spin, the VBM and CBM at either the K or K' point show Berry curvatures with opposite signs. Thus we get the reversal signs of the Berry curvature under ferroelectric polarization. The Berry curvatures of monolayer freestanding VSe_2 are shown in Figs. S5(a) and S5(b) [37], where we can find that the Berry curvatures around the K/K' valley hold different absolute values and exhibit opposite signs, and the absolute values are different from that of the case with the ferroelectric layer. To check whether the sign change of the Berry curvature of VSe_2 can be realized simply by applying the opposite vertical electrical field, we apply the vertical electrical fields with $+0.1$ and -0.1 eV/Å on it. We find that the signs of Berry curvature remain unchanged; see Figs. S6(a) and S6(b) [37]. Note that under an in-plane electric field, the carrier will obtain an anomalous velocity $v_a \sim E \times \Omega(k)$. For type- V_{up} (type- V_{dw}) states, by shifting the Fermi level between the K and K' valleys in the conduction (valence) bands, the spin-up electrons (holes) from the K valley move to the left (right) side of the sample under an in-plane electrical field, resulting in the net Hall current. Since the anomalous Hall conductivity is proportional to the integral of the Berry curvature over the Brillouin zone, the

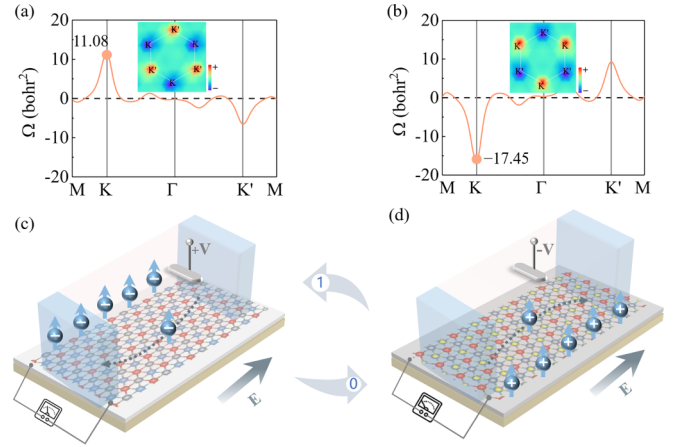


FIG. 4. Berry curvatures of (a) type- V_{up} configuration and (b) type- V_{dw} configuration along the high-symmetry points. Insets in (a), (b) show the contour maps of Berry curvatures over the 2D Brillouin zone. Diagrams of the anomalous valley Hall effect and memory devices in (c) type- V_{up} and (d) type- V_{dw} configurations. The holes/electrons are denoted by white $+/-$ symbols.

net Hall currents for the type- V_{up} and type- V_{dw} states are distinguishable by checking the deflection angle of the pointer in Figs. 4(c) and 4(d). Since the valley physics can be switched between the conduction and valence bands through ferroelectricity, we can realize the on-off switch of the valley physics in both the conduction (electron doping) and valence (hole doping) bands. Thus, the anomalous valley Hall effect is realized significantly and controlled effectively by ferroelectric switching.

To check whether the polarization direction in the VSe_2/Al_2S_3 heterostructure can be switched by an electric field, we apply an electric field (0.5 eV/Å) along the $-z$ direction on the type- V_{up} configuration. We find that its polarization is inverted after structural relaxation; see Fig. S7 [37]. Therefore, the polarization direction and then the valleytronics properties can be well controlled by electrostatic means, which can also be confirmed by some former studies [23–25,51,52].

The results have demonstrated that the VSe_2/Al_2S_3 heterostructure provides a promising opportunity for designing valleytronic memory devices. Here, we proposed a memory device prototype based on this heterostructure, shown in Figs. 4(c) and 4(d). The electric polarization in the Al_2S_3 is switched by a vertical external voltage. When polarization of the FE substrate is in the P_{up} configuration, the spin-up electrons accumulate in the left side of the VSe_2 monolayer due to the valley polarization at the CBM, resulting in a measurable transverse Hall voltage. Such state is identified as the “1” state of the device, as shown in Fig. 4(c). As the polarization direction of the FE substrate is reversed, spin-up holes become majority carriers, leading to different signal strength on transverse Hall voltage. This corresponds to the “0” state of the device, shown in Fig. 4(d). In this context, the data reading process is accessible by checking the FE coupling-induced signal strength differences with damage-free Hall voltage, thereby effectively avoiding the destructive effect caused by detecting the polarized states.

IV. CONCLUSION

In summary, through theoretical analysis, we propose a design principle for realizing reversible and nonvolatile control of the AVH effect. Using first-principles calculations and $k \cdot p$ model analysis, we further demonstrate that the AVH effect can be well tuned by stacking ferrovalley VSe_2 on FE monolayer Al_2S_3 . The sign of the transverse Hall voltage related to the AVH effect is strongly dependent on the FE polarization. The FE driven and tuning AVH effect in such multiferroic heterostructure offer a promising strategy for application in advanced all-electric data memory devices.

ACKNOWLEDGMENTS

We are grateful for the support from the National Natural Science Foundation of China (Grants No. 52171182 and No. 12104321), the “20 Clauses about Colleges and Universities (New)” Program of Jinan (Grant No. 202228107), the Key Research and Development Program of Shandong Province (Grant No. 2021ZLGX01), the Qilu Young Scholar Program of Shandong University, the Young Scholars Program of Shandong University, Shandong Provincial Qing Chuang Technology Support Plan (Grant No. 2021KJ002), and the HPC Cloud Platform of Shandong University.

-
- [1] K. F. Mak, D. Xiao, and J. Shan, Light–valley interactions in 2D semiconductors, *Nat. Photon.* **12**, 451 (2018).
- [2] D. Gunlycke and C. T. White, Graphene valley filter using a line defect, *Phys. Rev. Lett.* **106**, 136806 (2011).
- [3] D. Xiao, G. B. Liu, W. Feng, X. Xu, and W. Yao, Coupled spin and valley physics in monolayers of MoS_2 and other group-VI dichalcogenides, *Phys. Rev. Lett.* **108**, 196802 (2012).
- [4] H. Z. Lu, W. Yao, D. Xiao, and S. Q. Shen, Intervalley scattering and localization behaviors of spin-valley coupled Dirac fermions, *Phys. Rev. Lett.* **110**, 016806 (2013).
- [5] T. Cao, G. Wang, W. Han, H. Ye, C. Zhu, J. Shi, Q. Niu, P. Tan, E. Wang, B. Liu *et al.*, Valley-selective circular dichroism of monolayer molybdenum disulfide, *Nat. Commun.* **3**, 887 (2012).
- [6] S. Wu, J. S. Ross, G.-B. Liu, G. Aivazian, A. Jones, Z. Fei, W. Zhu, D. Xiao, W. Yao, D. Cobden *et al.*, Electrical tuning of valley magnetic moment through symmetry control in bilayer MoS_2 , *Nat. Phys.* **9**, 149 (2013).
- [7] A. Srivastava, M. Sidler, A. V. Allain, D. S. Lembke, A. Kis, and A. Imamoglu, Valley Zeeman effect in elementary optical excitations of monolayer WSe_2 , *Nat. Phys.* **11**, 141 (2015).
- [8] G. Aivazian, Z. Gong, A. M. Jones, R.-L. Chu, J. Yan, D. G. Mandrus, C. Zhang, D. Cobden, W. Yao, and X. Xu, Magnetic control of valley pseudospin in monolayer WSe_2 , *Nat. Phys.* **11**, 148 (2015).
- [9] X. Xu, W. Yao, D. Xiao, and T. F. Heinz, Spin and pseudospins in layered transition metal dichalcogenides, *Nat. Phys.* **10**, 343 (2014).
- [10] S. Manzeli, D. Ovchinnikov, D. Pasquier, O. V. Yazyev, and A. Kis, 2D transition metal dichalcogenides, *Nat. Rev. Mater.* **2**, 17033 (2017).
- [11] Y. Liu, Y. Gao, S. Zhang, J. He, J. Yu, and Z. Liu, Valleytronics in transition metal dichalcogenides materials, *Nano Res.* **12**, 2695 (2019).
- [12] D. Xiao, M.-C. Chang, and Q. Niu, Berry phase effects on electronic properties, *Rev. Mod. Phys.* **82**, 1959 (2010).
- [13] D. Xiao, W. Yao, and Q. Niu, Valley-contrasting physics in graphene: Magnetic moment and topological transport, *Phys. Rev. Lett.* **99**, 236809 (2007).
- [14] W. Y. Tong, S. J. Gong, X. Wan, and C. G. Duan, Concepts of ferrovalley material and anomalous valley Hall effect, *Nat. Commun.* **7**, 13612 (2016).
- [15] H. Hu, W.-Y. Tong, Y.-H. Shen, X. Wan, and C.-G. Duan, Concepts of the half-valley-metal and quantum anomalous valley Hall effect, *npj Comput. Mater.* **6**, 129 (2020).
- [16] Q. Cui, Y. Zhu, J. Liang, P. Cui, and H. Yang, Spin-valley coupling in a two-dimensional VSi_2N_4 monolayer, *Phys. Rev. B* **103**, 085421 (2021).
- [17] R. Li, J. Jiang, W. Mi, and H. Bai, Room temperature spontaneous valley polarization in two-dimensional $FeClBr$ monolayer, *Nanoscale* **13**, 14807 (2021).
- [18] X. Zhou, R.-W. Zhang, Z. Zhang, W. Feng, Y. Mokrousov, and Y. Yao, Sign-reversible valley-dependent Berry phase effects in 2D valley-half-semiconductors, *npj Comput. Mater.* **7**, 160 (2021).
- [19] R. Peng, Y. Ma, X. Xu, Z. He, B. Huang, and Y. Dai, Intrinsic anomalous valley Hall effect in single-layer Nb_3I_8 , *Phys. Rev. B* **102**, 035412 (2020).
- [20] W.-Y. Tong and C.-G. Duan, Electrical control of the anomalous valley Hall effect in antiferrovalley bilayers, *npj Quantum Mater.* **2**, 47 (2017).
- [21] T. Zhang, X. Xu, B. Huang, Y. Dai, and Y. Ma, 2D spontaneous valley polarization from inversion symmetric single-layer lattices, *npj Comput. Mater.* **8**, 64 (2022).
- [22] W. Du, R. Peng, Z. He, Y. Dai, B. Huang, and Y. Ma, Anomalous valley Hall effect in antiferromagnetic monolayers, *npj 2D Mater. Appl.* **6**, 11 (2022).
- [23] D. Zhang, Y. Zhang, and B. Zhou, Nonvolatile electrical control of valley splitting by ferroelectric polarization switching in a two-dimensional $AgBiP_2S_6/CrBr_3$ multiferroic heterostructure, *Nanoscale* **15**, 1718 (2023).
- [24] B. Marfoua and J. Hong, Reversal of anomalous Hall conductivity by perpendicular electric field in 2D WSe_2/VSe_2 heterostructure, *Commun. Phys.* **5**, 266 (2022).
- [25] R. J. Sun, R. Liu, J. J. Lu, X. W. Zhao, G. C. Hu, X. B. Yuan, and J. F. Ren, Reversible switching of anomalous valley Hall effect in ferrovalley Janus $1T-CrOX$ ($X = F, Cl, Br, I$) and the multiferroic heterostructure $CrOX/In_2Se_3$, *Phys. Rev. B* **105**, 235416 (2022).
- [26] W. Kohn and L. J. Sham, Self-consistent equations including exchange and correlation effects, *Phys. Rev.* **140**, A1133 (1965).
- [27] G. Kresse and J. Furthmüller, Efficient iterative schemes for *ab initio* total-energy calculations using a plane-wave basis set, *Phys. Rev. B* **54**, 11169 (1996).
- [28] J. P. Perdew, A. Ruzsinszky, G. I. Csonka, O. A. Vydrov, G. E. Scuseria, L. A. Constantin, X. Zhou, and K. Burke, Restoring the density-gradient expansion for exchange in solids and surfaces, *Phys. Rev. Lett.* **100**, 136406 (2008).

- [29] J. P. Perdew, K. Burke, and M. Ernzerhof, Generalized gradient approximation made simple, *Phys. Rev. Lett.* **77**, 3865 (1996).
- [30] P. E. Blöchl, Projector augmented-wave method, *Phys. Rev. B* **50**, 17953 (1994).
- [31] G. Kresse and D. Joubert, From ultrasoft pseudopotentials to the projector augmented-wave method, *Phys. Rev. B* **59**, 1758 (1999).
- [32] H. J. Monkhorst and J. D. Pack, Special points for Brillouin-zone integrations, *Phys. Rev. B* **13**, 5188 (1976).
- [33] J. Heyd and G. E. Scuseria, Assessment and validation of a screened Coulomb hybrid density functional, *J. Chem. Phys.* **120**, 7274 (2004).
- [34] J. Neugebauer and M. Scheffler, Adsorbate-substrate and adsorbate-adsorbate interactions of Na and K adlayers on Al(111), *Phys. Rev. B* **46**, 16067 (1992).
- [35] S. Grimme, Semiempirical GGA-type density functional constructed with a long-range dispersion correction, *J. Comput. Chem.* **27**, 1787 (2006).
- [36] A. A. Mostofi, J. R. Yates, G. Pizzi, Y.-S. Lee, I. Souza, D. Vanderbilt, and N. Marzari, An updated version of WANNIER90: A tool for obtaining maximally-localised Wannier functions, *Comput. Phys. Commun.* **185**, 2309 (2014).
- [37] See Supplemental Material at <http://link.aps.org/supplemental/10.1103/PhysRevB.108.155431> for the crystal structures and band structures of monolayer VSe₂ and Al₂S₃, the six stacking configurations of the VSe₂/Al₂S₃ heterostructures, the spin-polarized charge densities of type-V_{up} and type-V_{dw} with FM and AFM configurations, the Berry curvatures of monolayer VSe₂, the crystal structure of VSe₂/Al₂S₃ heterostructures under an external electric field, the energies and interlayer distances of the VSe₂/Al₂S₃ heterostructures, the energy difference ΔE between the AFM and FM states of VSe₂/Al₂S₃ heterostructures, and the fitting results from first-principles band structure calculations around the *K* and *K'* points.
- [38] X. Wang, D. Li, Z. Li, C. Wu, C. M. Che, G. Chen, and X. Cui, Ferromagnetism in 2D vanadium diselenide, *ACS Nano* **15**, 16236 (2021).
- [39] M. Wu, Two-dimensional van der Waals Ferroelectrics: Scientific and technological opportunities, *ACS Nano* **15**, 9229 (2021).
- [40] D. Zhang, P. Schoenherr, P. Sharma, and J. Seidel, Ferroelectric order in van der Waals layered materials, *Nat. Rev. Mater.* **8**, 25 (2022).
- [41] C. F. Fu, J. Sun, Q. Luo, X. Li, W. Hu, and J. Yang, Intrinsic electric fields in two-dimensional materials boost the solar-to-hydrogen efficiency for photocatalytic water splitting, *Nano Lett.* **18**, 6312 (2018).
- [42] W. Ding, J. Zhu, Z. Wang, Y. Gao, D. Xiao, Y. Gu, Z. Zhang, and W. Zhu, Prediction of intrinsic two-dimensional ferroelectrics in In₂Se₃ and other III₂-VI₃ van der Waals materials, *Nat. Commun.* **8**, 14956 (2017).
- [43] F. Xue, W. Hu, K. C. Lee, L. S. Lu, J. Zhang, H. L. Tang, A. Han, W. T. Hsu, S. Tu, W. H. Chang *et al.*, Room-temperature ferroelectricity in hexagonally layered α -In₂Se₃ nanoflakes down to the monolayer limit, *Adv. Funct. Mater.* **28**, 1803738 (2018).
- [44] A. Xie, H. Hao, C.-S. Liu, X. Zheng, L. Zhang, and Z. Zeng, Giant tunnel electroresistance in two-dimensional ferroelectric tunnel junctions constructed with a Sc₂CO₂/In₂Se₃ van der Waals ferroelectric heterostructure, *Phys. Rev. B* **107**, 115427 (2023).
- [45] K. L. Seyler, D. Zhong, B. Huang, X. Linpeng, N. P. Wilson, T. Taniguchi, K. Watanabe, W. Yao, D. Xiao, M. A. McGuire *et al.*, Valley manipulation by optically tuning the magnetic proximity effect in WSe₂/CrI₃ heterostructures, *Nano Lett.* **18**, 3823 (2018).
- [46] Z. He, R. Peng, X. Feng, X. Xu, Y. Dai, B. Huang, and Y. Ma, Two-dimensional valleytronic semiconductor with spontaneous spin and valley polarization in single-layer Cr₂Se₃, *Phys. Rev. B* **104**, 075105 (2021).
- [47] C. Lei, X. Xu, T. Zhang, B. Huang, Y. Dai, and Y. Ma, Nonvolatile controlling valleytronics by ferroelectricity in 2H-VSe₂/Sc₂CO₂ van der Waals heterostructure, *J. Phys. Chem. C* **125**, 2802 (2021).
- [48] A. Kormányos, V. Zólyomi, N. D. Drummond, P. Rakyta, G. Burkard, and V. I. Fal'ko, Monolayer MoS₂: Trigonal warping, the Γ valley, and spin-orbit coupling effects, *Phys. Rev. B* **88**, 045416 (2013).
- [49] X. Ma, X. Shao, Y. Fan, J. Liu, X. Feng, L. Sun, and M. Zhao, Tunable valley splitting and anomalous valley Hall effect in VTe₂/Ga₂S₃ heterostructures, *J. Mater. Chem. C* **8**, 14895 (2020).
- [50] D. J. Thouless, M. Kohmoto, M. P. Nightingale, and M. den Nijs, Quantized Hall conductance in a two-dimensional periodic potential, *Phys. Rev. Lett.* **49**, 405 (1982).
- [51] W. Luo, K. Xu, and H. Xiang, Two-dimensional hyperferroelectric metals: A different route to ferromagnetic-ferroelectric multiferroics, *Phys. Rev. B* **96**, 235415 (2017).
- [52] Y. Feng, T. Zhang, Y. Dai, B. Huang, and Y. Ma, *p*-orbital multiferroics in single-layer SiN, *Appl. Phys. Lett.* **120**, 193102 (2022).